Supplementary information

Kinetic and structural properties of a robust bacterial L-amino acid oxidase

Simone Savino, J. Daniël-Morah Meijer, Henriëtte J. Rozeboom, Hugo L. van Beek, Marco W. Fraaije

Sequence of recombinantly expressed LAAO

>*Pl*-LAAO

MGSSHHHHHHSSGLVPRGSHMTHYTFGKEITDKQLPSQVKVAIVGAGMSGLYSAW
RLQQEANCQDLAIFERSDRTGGRLDSDLIEFKNLRSDEPKTITVKEEQGGMRFLFDG
MDDLMALFLKLNLQDDIVPFPMNSGGNNRLFFRGESFSVSDAQQDDYAIWSHLYNL
DQSEQGVNPKDIVNVVFNRILEANPQFQQRPKVRGPQFWQDFRLECQWKGQGLNQ
WTLWDLYTDMGYSQECITMLYRVLGFNGTFLSQMNAGVAYQLLEDFPAGVKFKTF
KDGFSTLPNKLVEEVGTNNIHLQTTIEEIDFNEESGLYELSYAHIDAHGKIHKGLVKA
EKVILGLPRLALEKLFVRSNVINRLDQDRSELLWNTLQSASNQPLLKINLYYDSAWW
GRGTTGRPAVEFGPNFADLPTGSVYPFYAVNEELAAALMYEERTTHPSDAVEAKLE
RIGNDKYERPAALTIYCDYLNINFWSNLQNIGETYHNPKQDHYVENVPDDIYPASTA
VVEQATRFFKDIFNTHYVPAPVLTSARIWEGSVKFDIPANRQFGYGVHQWAVGAND
KEVMATLSEPLPNLFTCGEAFSDYQGWVEGALRSTDLALEKGFGLKPLSQAYFESTH
ISSSDAIKAVYEENSSKLINQYIETNFAASAAPIEKADDEQSVIGVNLSYFDVK

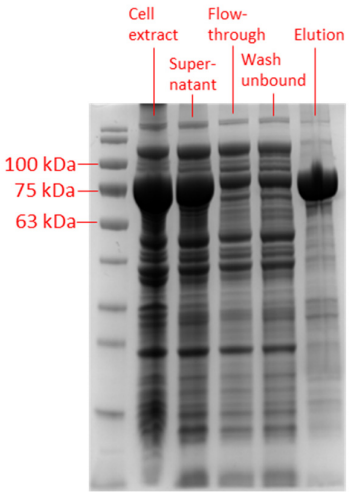

Figure S1: SDS-PAGE of the LAAO purification process.

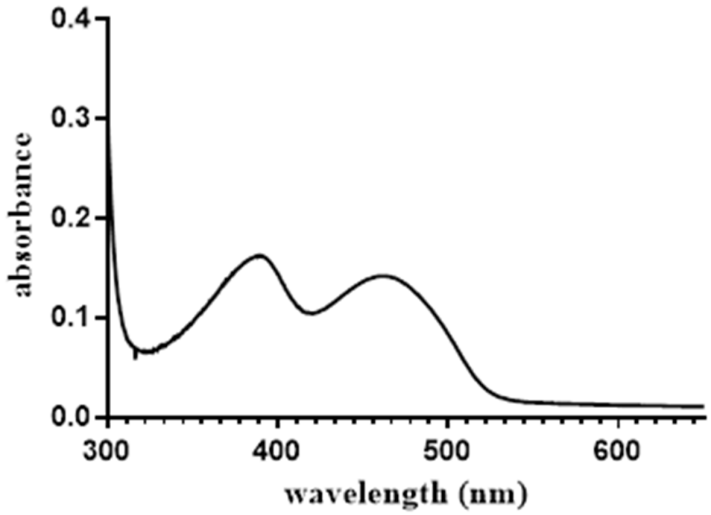

Figure S2: UV-Vis absorbance spectrum of purified LAAO.

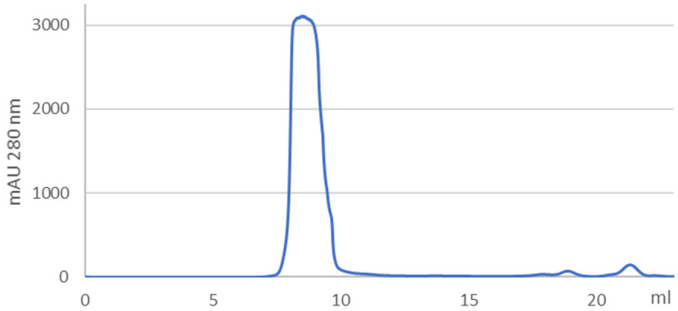

Figure S3: Size exclusion chromatogram of LAAO sample before crystallisation experiments. The sample was collected in small fractions and pooled together, avoiding the shoulder on the right side of the peak.

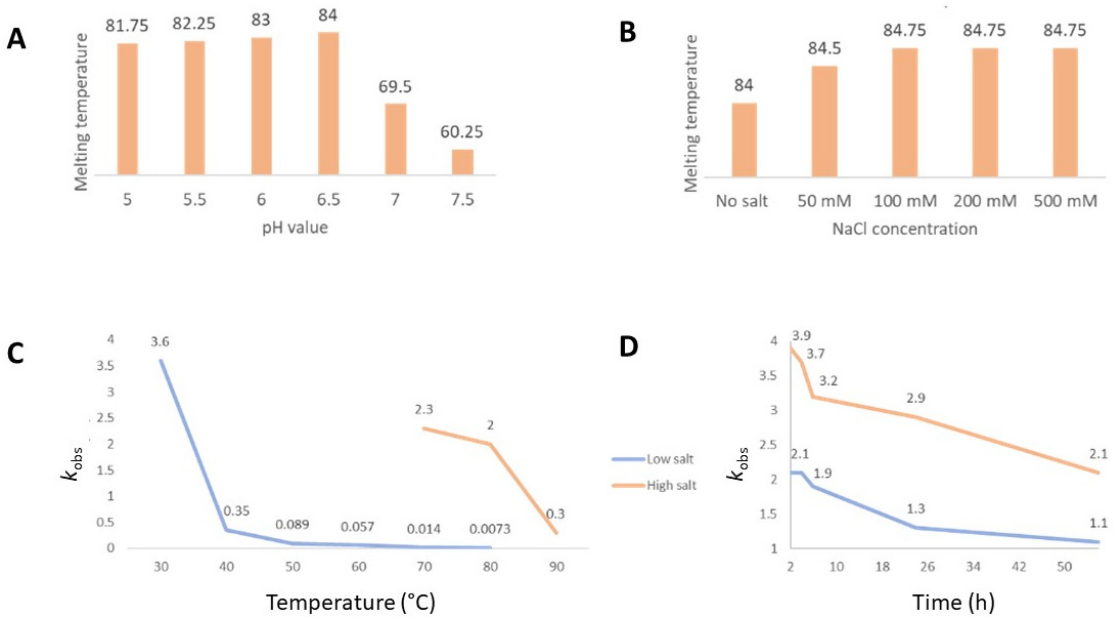

Figure S4. (A) pH-dependence of T_m of *Pl*-LAAO in 50 mM TRIS/Cl at different pH values, (B) salt concentration dependence of T_m of *Pl*-LAAO in 50 mM TRIS/Cl, pH 6.5, with different NaCl concentrations, (C) observed *Pl*-LAAO activity after 10 min incubation at different temperature, (D) observed *Pl*-LAAO activity upon incubation at 37 ºC.

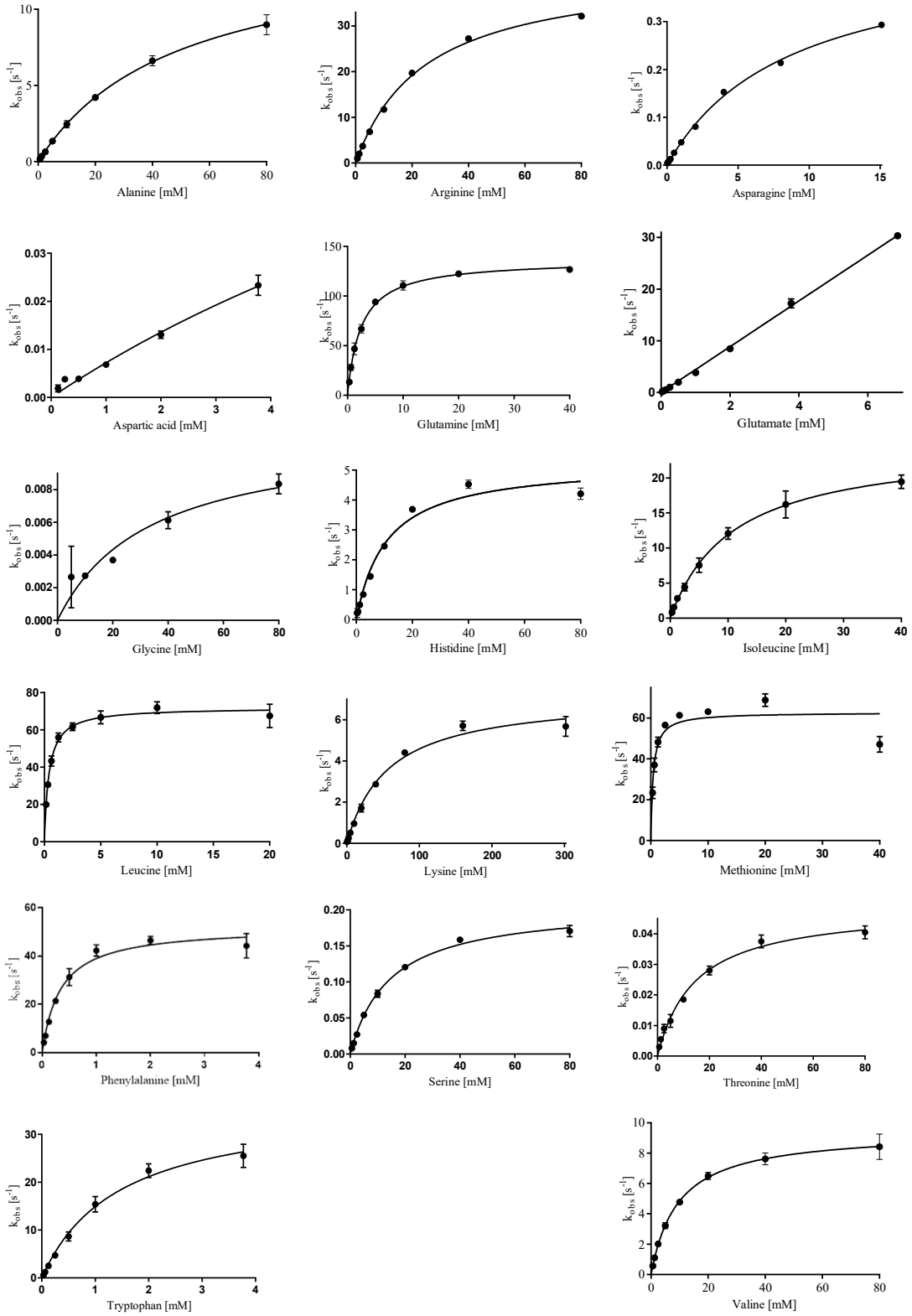

Figure S5: Steady state kinetics for 18 of the 20 proteinogenic amino acids. All measurements were performed in duplicate. No activity was observed for proline and cysteine.

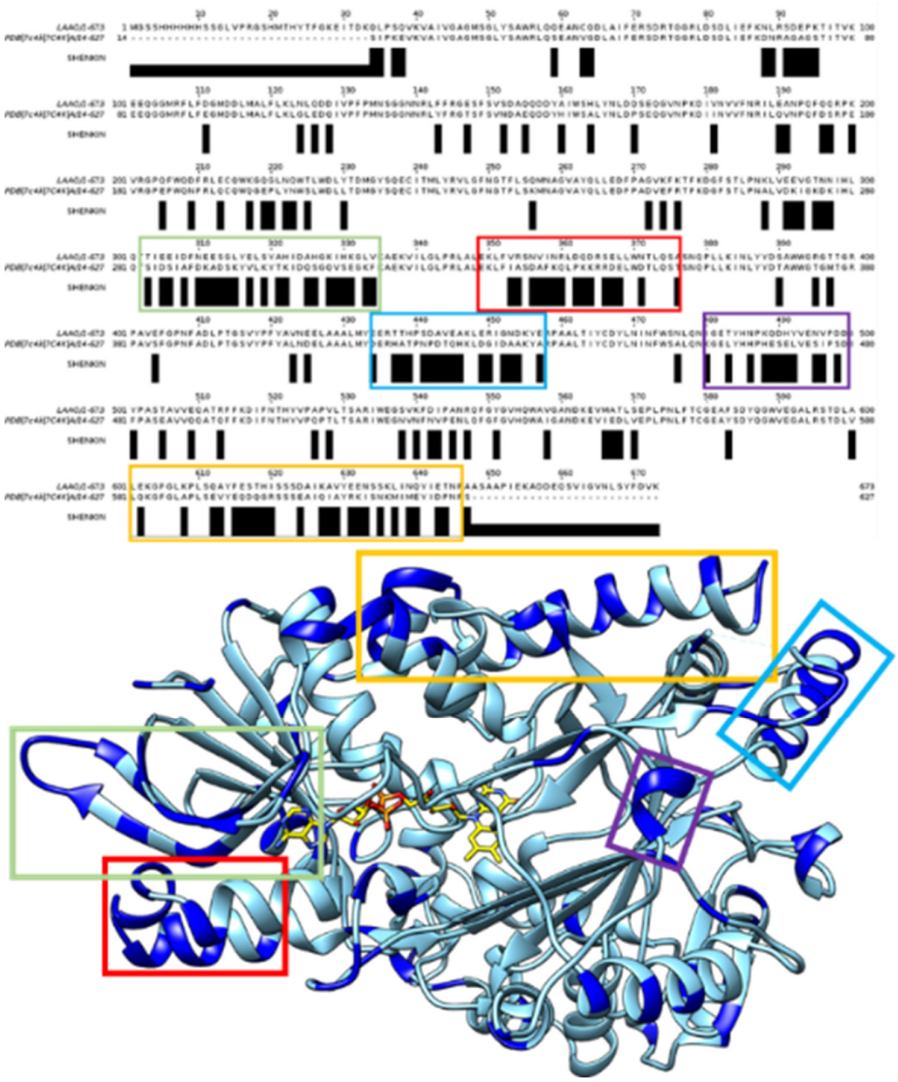

Figure S5: Top, sequence alignment between *Pl*-LAAO and the homologue from ancestral sequence reconstruction, the structure of which is deposited under the PDB 7C4K. Non-conserved sites are highlighted by black bars. Bottom, the structure of 7C4K with non-conserved sites in dark blue. All of these are limited to surface exposed portions of the protein, while the active site and the cofactor binding residues are fully retained. For sake of clarity, the portions with highest divergence are reported in rectangles of the same colour in both sequence alignment and structure representation.

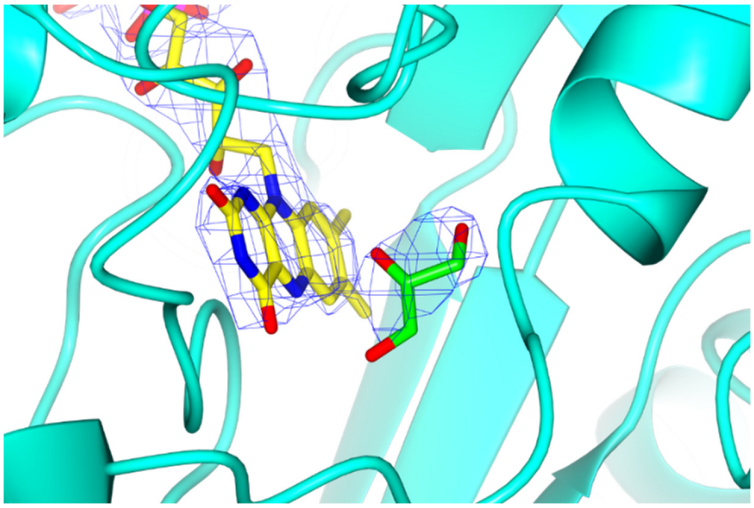

Figure S6: Focus on the electron density (in blue chicken wire) of FAD in yellow carbons and glycerol in green carbons present only in molecule B of the asymmetric unit.

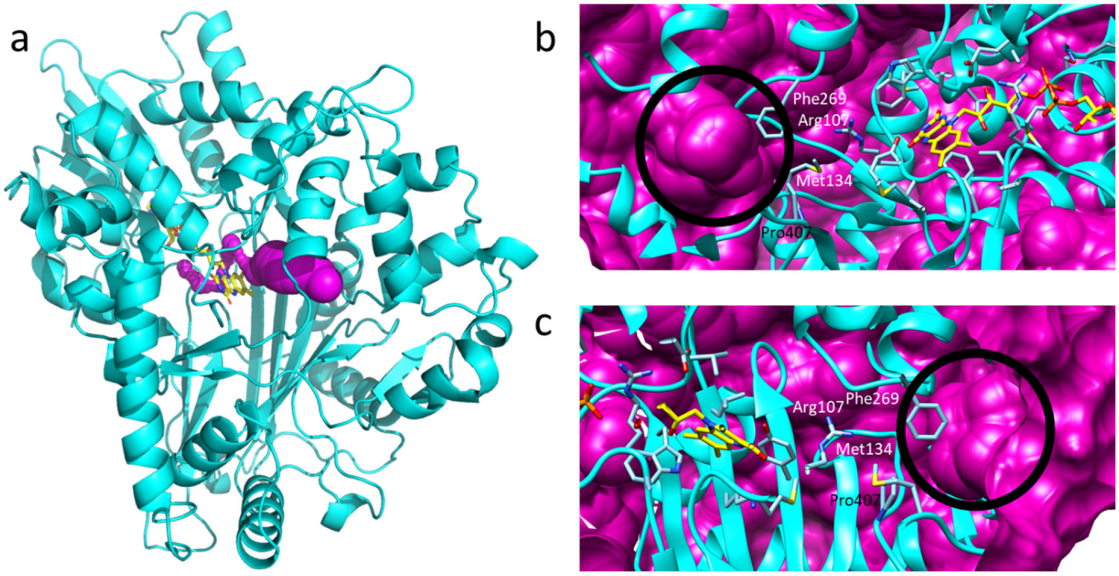

Figure S7: a) Structure of LAAO with the tunnel (magenta) leading from the FAD cofactor to the solvent-accessible surface. b) Side view of the tunnel, the entrance of which is enclosed in the black circle. A set of side chains, the motion of which is necessary to allow access to the active site, is highlighted. c) A 180° rotated view of the same side view.

Table S1: Crystallographic data collection and refinement statistics. The values for the high-resolution shell are shown in parenthesis.

Data collection	**PDB 7OG2**
Wavelength (Å)	0.96862
Space group	I222
Molecules in A.U.	2
No. of unique reflections	38863 (4684)
Cell dimensions: *a*, *b*, *c* (Å)	92.0 134.2 251.9
Resolution (Å)	47.2 - 2.8 (2.87-2.80)
R_{sym} or R_{merge} (%)	13.4 (84.6)
R_{pim} (%)	6.0 (37.7)
$I / \sigma I$	8.3 (2.0)
$CC_{1/2}$	0.995 (0.824)
Completeness (%)	100.0(100.0)
Redundancy	6.7 (6.6)
Refinement	
R_{work} / R_{free}	19.8 / 26.1
No. atoms	
Protein	9870
Ligand	2 x FAD & 1 x GOL
Water	99
Ions	1 Pt^{2+} & 7 Cl^{-}
R.m.s. deviations	
Bond lengths (Å)	0.0103
Bond angles (°)	1.65
Ramachandran statistics (%)	
favored	95.67
allowed	3.92
outliers	0.41